


Interactions and Mobility Edges: Observing the Generalized Aubry-André ModelFangzhao Alex An,^{1,*†} Karmela Padavić,^{1,*} Eric J. Meier,¹ Suraj Hegde,² Sriram Ganeshan,^{3,4,‡}
J. H. Pixley,^{5,§} Smitha Vishveshwara,^{1,||} and Bryce Gadway^{1,¶}¹*Department of Physics, University of Illinois at Urbana-Champaign, Urbana, Illinois 61801-3080, USA*²*Max-Planck Institute for Physics of Complex Systems, 01187 Dresden, Germany*³*Physics Department, City College of the CUNY, New York, New York 10031, USA*⁴*CUNY Graduate Center, New York, New York 10031, USA*⁵*Department of Physics and Astronomy, Center for Materials Theory, Rutgers University, Piscataway, New Jersey 08854, USA* (Received 15 July 2020; revised 4 December 2020; accepted 8 January 2021; published 29 January 2021)

Using synthetic lattices of laser-coupled atomic momentum modes, we experimentally realize a recently proposed family of nearest-neighbor tight-binding models having quasiperiodic site energy modulation that host an exact mobility edge protected by a duality symmetry. These one-dimensional tight-binding models can be viewed as a generalization of the well-known Aubry-André model, with an energy-dependent self-duality condition that constitutes an analytical mobility edge relation. By adiabatically preparing low and high energy eigenstates of this model system and performing microscopic measurements of their participation ratio, we track the evolution of the mobility edge as the energy-dependent density of states is modified by the model's tuning parameter. Our results show strong deviations from single-particle predictions, consistent with attractive interactions causing both enhanced localization of the lowest energy state due to self-trapping and inhibited localization of high energy states due to screening. This study paves the way for quantitative studies of interaction effects on self-duality induced mobility edges.

DOI: [10.1103/PhysRevLett.126.040603](https://doi.org/10.1103/PhysRevLett.126.040603)

Disorder-induced localization of quantum mechanical wave functions represents a fundamental change in the nature of eigenstates [1]. Analog simulators based on photonic materials [2] and ultracold atoms [3] have opened up new possibilities for exploring localization phenomena in coherent and controllable settings. Some of the earliest observations of localization for both light [4] and atoms [5,6] were achieved with deterministic quasiperiodic potentials in the Aubry-André (AA) model [7–10]. However, the AA model is rather fine-tuned and does not manifest a mobility edge, i.e., energy-dependent localization transition that separates localized states from extended ones as a function of energy. Mobility edges are expected to be the generic behavior of more general quasiperiodic models in one [11–22] and higher dimensions [23–27], and also accompany the appearance of delocalized states for models with short-range disorder in higher dimensions [28].

Recently, mobility edges (MEs) in noninteracting models have been observed in three-dimensional disordered systems [29–32], as well as in reduced dimensions with quasiperiodicity in experiments based on ultracold atoms [33–35]. In these cases, however, accurate experimental control over the location of the mobility edge is lacking, as its analytic functional form is unknown. It is in principle possible to circumvent this issue in quasiperiodic systems by exploiting tight-binding models that have an exact mobility edge that can be derived from an energy dependent

self-duality condition (i.e., the discrete Schrödinger equation maps back onto itself upon a series of weighted Fourier transforms from real to momentum space) [13–15,17,36–39]. Experimental realization of an analytical mobility edge can help resolve the effects of interactions on the energy dependent localization transition [18,20,37,39], which remains a subtle and open theoretical question.

In this work, we experimentally realize a generalized Aubry-André (GAA) model that has an exact mobility edge [36] and demonstrate control over the ME physics by employing synthetic lattices of laser-coupled atomic momentum modes [40,41]. Crucially, in the absence of interactions this model has an energy dependent self-duality that gives rise to the mobility edge. In experiment, we probe the presence of the ME by measuring the localization properties of the low and high energy states of the system, and vary the energy of the ME via a tuning parameter. We map out localization phase diagrams for these energy states, demonstrating that the ME is shifted by atomic interactions but that overall the localization transitions and the ME survive. Our work showcases the capacity of cold atoms for the exploration of localization, MEs, and interactions in quasiperiodic lattice models.

The Hamiltonian realized in this work, $H_{\text{tot}} = H_{\text{GAA}} + H_{\text{int}}$, involves both the tight-binding GAA model proposed in Ref. [36] and a contribution due to atomic interactions. The GAA Hamiltonian is

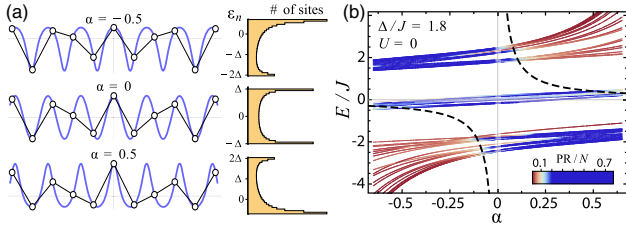


FIG. 1. The generalized self-dual Aubry-André model. (a) The generalized Aubry-André potential and lattice site energies of Eq. (2) shown for $\phi = 0$ and tuning parameter $\alpha = -0.5, 0, 0.5$, with corresponding distributions of lattice site energies ϵ_n . (b) Calculated eigenenergies and participation ratios (PRs, in color) vs α for a noninteracting model just below the critical quasiperiodicity strength at $\Delta/J = 1.8$ ($N = 51$ sites). Away from $\alpha = 0$, eigenstates localize at different energies, forming a mobility edge. Dashed black lines show analytically predicted energy values of the ME [Eq. (3)].

$$H_{\text{GAA}} = -J \sum_n (c_{n+1}^\dagger c_n + \text{H.c.}) + \sum_n \epsilon_n c_n^\dagger c_n, \quad (1)$$

where J is a nearest-neighbor tunneling amplitude, c_n destroys a boson at site n , and the GAA quasiperiodic site energies read

$$\epsilon_n = \Delta \frac{\cos(2\pi n b + \phi)}{1 - \alpha \cos(2\pi n b + \phi)}, \quad (2)$$

with quasiperiodicity amplitude and phase given by Δ and ϕ , respectively. We choose $b = (\sqrt{5} - 1)/2$, though the localization results we present here hold for any irrational number [36]. The tuning parameter $\alpha \in (-1, 1)$ controls the shape of the potential and the distribution of site energies, as shown in Fig. 1(a). At $\alpha = 0$, Eq. (2) reduces to the standard AA form, with a cosine dispersion and cosine distribution of site energies leading to an energy-independent localization transition. For $\alpha \neq 0$, the GAA model exhibits an exact ME at energy E following the relationship [36]

$$\alpha E = 2J - \Delta, \quad (3)$$

for the positive J and Δ values we consider. For GAA Hamiltonian eigenstates satisfying Eq. (3), the corresponding Schrödinger equation is invariant under a series of weighted Fourier transforms between real and momentum space (i.e., self-dual), which implies the eigenstates are not localized in either basis and are thus critical.

Atomic interactions enrich the physics of this system. Low energy s -wave collisions between atoms in the momentum modes [42] are described by $H_{\text{int}} = (U/2N_{\text{at}}) \sum_{i,j,k,l} c_i^\dagger c_j^\dagger c_k c_l$. Here $U = g\rho$ is the mean-field interaction energy per atom for a sample of N_{at} atoms occupying a single mode, ρ is the atomic number density, $g = 4\pi\hbar^2 a/M$ is the interaction term, M is the atomic mass, and a is the scattering length. Here, we consider a

approximate description of the interactions [43], treating them with a mean-field Gross-Pitaevskii formalism that considers the interactions as an effectively local intramode attraction with a collective energy scale U . We find that this treatment, while ignoring some details [43], provides a simple mean-field-level comparison that captures most of the salient features.

To probe the expected ME of this system, we determine the localization properties of the GAA eigenstates. We quantify localization through the participation ratio, $\text{PR} = 1/\sum_n P_n^2$, where P_n is the normalized atom population at site n . The PR effectively counts the number of sites that “participate” in hosting a state. It ranges from $\text{PR} \sim N$ in the extended regime to $\text{PR} = 1$ for states localized to a single site. For $\alpha \neq 0$, states on opposite sides of the ME correspond to PRs close to opposite extremes of this range [see Fig. 1(b)].

The strong dependence of localization behavior on α can be understood by considering how this parameter influences the site energy distribution [see Fig. 1(a)]. For $\alpha < 0$, the site-energy distribution is weighted towards higher energy values. In a heuristic picture, more sites “sit” on top of potential wells rather than at their bottoms. Thus, for negative α , a higher (lower) quasiperiodicity strength is required to induce localization for states at high (low) energy, as there are many more (fewer) nearby sites to which they can resonantly hop. For positive values of α , the complete opposite behavior is found, with the localization behavior of the high and low energy states swapped. In this way the ME is directly controllable through the parameter α , as suggested by Eq. (3).

We experimentally realize the GAA model with control over α in a synthetic lattice [47] of coupled atomic momentum modes [40,41]. We start with an optically trapped Bose-Einstein condensate of $\sim 10^5$ ^{87}Rb atoms. We then use a pair of counterpropagating lasers (wavelength $\lambda = 1064$ nm) to drive Bragg transitions that can change the atomic momentum in increments of $2\hbar k$ (with $k = 2\pi/\lambda$ and \hbar the reduced Planck’s constant). While one of the lasers has a single frequency, the other beam is engineered to have many distinct components. Together, these lasers drive a set of two-photon Bragg transitions that create effective “tunneling links” between the synthetic lattice “sites” (relating physically to modes with momenta $p_n = 2n\hbar k$, with n the site index). By independently tuning the strength, phase, and detuning for each of the Bragg transitions, we respectively control the tunneling amplitude, tunneling phase, and site-to-site energy difference of each link in the synthetic lattice. Here, we make use of the generic site energy control to exactly implement the GAA potential of Eq. (2) on a 21-site lattice for $|\alpha| \leq 0.5$ [43]. The direct measurement of populations at each synthetic lattice “site” is achieved by performing absorption imaging after a time-of-flight period.

To explore the presence of a ME, we seek to adiabatically prepare the low and high energy eigenstates of the system. We initialize population in the central site of a lattice with all tunneling links set to 0 and with GAA site energies imposed. The phase term of Eq. (2) is set to be $\phi = \pi$ (0) to ensure that the initial lattice site has the lowest (highest) energy. We linearly ramp up the tunneling from 0 to a final value of $J/h = 625$ Hz over 0.75 ms, and hold at that value for 1.25 ms. At the single-particle level and in its adiabatic limit, this ramping procedure prepares the lowest (highest) energy eigenstate of the full Hamiltonian when initializing at the lowest (highest) energy site in the zero-tunneling limit [43]. As shown in Figs. 2(a) and 2(b), this ramp can be viewed as tuning the system from the limit of infinite quasiperiodicity ($\Delta/J = \infty$, where our initialized state maps to a localized eigenstate), to a final Δ/J ratio.

This procedure is expected to be robust in the insulating regime and absent interactions. For our 0.75 ms ramp, diabatic corrections become important as the eigenstates

hybridize upon encountering a delocalization transition. While the loading procedure does not faithfully prepare the eigenstates in the metallic regime, it is well suited to determining the delocalization transition in the absence of interactions [43]. Interactions change this picture slightly: for the GS and for the ES when $\alpha \gtrsim 0$, the initialization and ramping procedures remain mostly intact, with only slight nonadiabaticities introduced [43]. Our preparation of the lowest energy eigenstate, or GS, is robust to the presence of atomic interactions. In contrast, our single-site preparation does not capture the effect of screening for the ES, and in practice our prepared ES is in fact a distribution of high energy eigenstates.

Figure 2(a) demonstrates this procedure performed for the highest energy state of the canonical AA model ($\alpha = 0$), demonstrating localization above the critical quasiperiodicity strength $(\Delta/J)_c = 2$ and extended delocalization below it. By studying the localization properties of samples initiated to prepare the lowest and highest energy eigenstates (ground state denoted ‘‘GS’’ and highest excited state denoted ‘‘ES’’), we expect to find evidence of an energy-dependent localization transition when $\alpha \neq 0$. The numerically calculated PR values of the eigenstates in the non-interacting limit for $\alpha = -0.5$ are shown in Fig. 2(b). They illustrate a clear energy dependence in agreement with the prediction of Eq. (3) (dashed black line), with the GS and ES localization transitions found near $\Delta/J = 1$ and $\Delta/J = 3$, respectively.

The experiment features interactions that can shift the localization transitions away from single-particle predictions. We capture this numerically by solving the Gross-Pitaevskii equation (GPE) for a homogeneous mean-field interaction energy of $U/h = 300$ Hz ($U/J = 0.48$ in terms of the final tunneling value) [43]. Interacting GPE simulations of the PR values are shown in Fig. 2(c) as the dashed blue (yellow) lines for the GS (ES), accounting for the exact experimental parameter ramp (with $U = 0$ solid-line curves included for comparison).

Figure 2(c) shows the energy-dependent localization behavior for $\alpha = -0.5$. We plot the normalized PR values, PR/N , which should range from $1/21$ (gray horizontal line) in the site-localized limit to $\lesssim 2/3$ in the extended regime. We observe PR/N values that remain low for a range of large Δ/J values, giving way to a sharp increase as the states delocalize. To note, the experimental PR/N measurements do not reach the expected value of $2/3$ deep in the metallic regime. This is likely due to a combination of diabatic effects associated with the ramp (included in the simulation curves) as well as decoherence between the momentum modes due to spatial separation. Still, from the distinct separation of the measured localization transitions for the GS and ES we can infer the existence of an intervening ME.

Consistent with the GPE simulations, we do not observe a significant influence of interactions for $\alpha = -0.5$. The

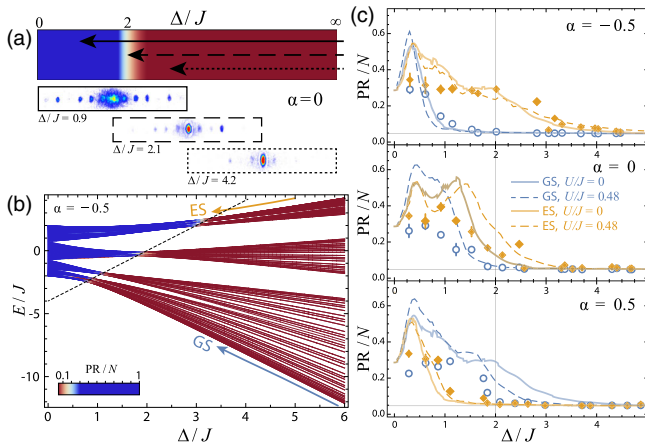


FIG. 2. Probing localization by adiabatic Hamiltonian evolution. (a) Cartoon of the experimental sequence. Atoms initially localized for $\Delta/J = \infty$ are slowly loaded into an eigenstate of the GAA model at a final quasiperiodicity-to-tunneling ratio Δ/J . Bar color relates to the normalized participation ratio [see color bar inset in (b)], for $\alpha = 0$ and no interactions. Bottom: atomic momentum distributions, corresponding to populations in the synthetic lattice, of the ES for $\alpha = 0$ in the localized regime ($\Delta/J = 4.2$), near the delocalization transition ($\Delta/J = 2.1$), and in the delocalized regime ($\Delta/J = 0.9$). (b) Numerically calculated PRs overlaid on the eigenenergies of the GAA model for $\alpha = -0.5$, $\phi = \pi$, and $N = 201$ sites. High-energy states localize at larger quasiperiodicity strengths than low-energy states, highlighting the presence of the mobility edge of Eq. (3) (dashed black line). The colors of the energy curves relate to states' PR/N values, according to the inset color bar. (c) PR/N vs Δ/J for GS (open blue circles) and ES (yellow diamonds) under $\alpha = -0.5, 0, 0.5$. Numerical curves incorporate the exact experimental tunneling ramp and assume a mean-field energy $U/J = 0.48$ ($U/h = 300$ Hz) for the dashed curves and zero interactions ($U/J = 0$) for the solid curves. Error bars in (c) denote one standard error of the mean.

$\alpha = 0$ case reduces to the standard AA model. Thus, in the absence of interactions, all eigenstates should delocalize at the same critical value of $\Delta/J = 2$. However, we observe in Fig. 2(c) that the transition splits for the lowest and highest energy states, signaling a mobility edge that arises solely from atomic interactions [48]. For $\alpha = +0.5$ [Fig. 2(c)], our data show an inversion of the mobility edge: the excited state localizes at a weaker quasiperiodicity amplitude than the ground state. This inversion is expected due to a symmetry of the noninteracting Hamiltonian (H_{GAA}), which exchanges the lowest and the highest energy states as $\alpha \rightarrow -\alpha$ (and $\phi \rightarrow \phi + \pi$ for an exact inversion in a finite system). For $\alpha = +0.5$, we also observe a shift of the GS localization transition away from the $U = 0$ theory prediction.

We find qualitative agreement with the behavior expected based on the GAA model, observing a ME that inverts as we go from $\alpha = -0.5$ to $\alpha = +0.5$. However, we do not observe the simple symmetry between the GS and ES predicted by the GAA model [Eq. (2)] as α changes sign. Instead, we find an asymmetric response, with a larger magnitude of separation between the GS and ES transitions for $\alpha = +0.5$ as compared to $\alpha = -0.5$ and the appearance of a mobility edge even for the $\alpha = 0$ case. These observations are consistent with interaction-driven shifts of the transitions and the fact that the interacting GAA model has an enlarged symmetry, by which the GS and ES localization properties exchange if we take $U \rightarrow -U$ as $\alpha \rightarrow -\alpha$. These results demonstrate that, despite interactions strongly breaking the self-dual symmetry of the noninteracting model, the ME is renormalized and survives interactions.

Our simple mean-field description of the system's effectively local and attractive interactions [42,43,49] allows us to provide an intuitive picture for how the localization properties of the GS and ES are, respectively, affected. For states at low energy, the interaction-induced chemical potential shifts inhibit delocalization in the synthetic lattice. This instability towards self-trapping for attractive interactions [50] shifts the ground state localization transition towards lower quasiperiodicity strengths for all values of α . In contrast, for states at high energy, attractive interactions can effectively screen the GAA quasiperiodic potential, thus promoting delocalization [50,51].

Figure 3 provides a more comprehensive picture for the localization behavior of the interacting GAA model, achieved by studying the GS and ES localization transitions for a larger set of α values. For the GS and ES, we perform the same preparation ramps as described for Fig. 2, starting from the $\Delta/J = \infty$ limit. For each sampled α value, we determine the “critical” Δ/J at which delocalization occurs, relating to an increase of the normalized participation ratio (PR/ N) above a threshold value set to 0.19 [43]. The collections of critical Δ/J values, shown

respectively as open (white) diamonds and black disks for the ES and GS, serve to define the localization-delocalization boundaries for these states.

In the absence of interactions, these two curves should be symmetric about an inversion of $\alpha \rightarrow -\alpha$, with a crossing at $\alpha = 0$ that relates to the absence of a ME in the canonical AA model. The interactions modify this picture, however. The crossing of these localization transition lines is shifted away from $\alpha = 0$ to $\alpha \sim 0.3$ – 0.4 . This is in agreement with the expectations from the interaction phenomena of self-trapping and screening.

Beneath the data, we show the simulated difference in PR/ N for the ideal GS and ES with interactions ($U = 0.48J$) [52]. This difference of the participation ratios reveals a behavior similar to what is observed in experiment, such as a shift of the crossing point away from $\alpha = 0$. It also indicates a region at large Δ/J in which both states are insulating and a region at small Δ/J in which both states are metallic. Finally, it shows two regions in which mobility edges can be directly inferred based on the localization of only one of these states.

We note that, while we find fair agreement between the observed GS localization boundary and the predicted behavior of the true lowest energy eigenstate, there is considerable deviation of the experimental ES result. This discrepancy results from nonideal ES initialization due to the influence of interactions. In short, our procedure of preparing eigenstates by initializing population at a single site in the $\Delta/J = \infty$ limit works ideally when there are no interactions. It continues to work for the GS when effectively attractive interactions are considered. For the highest energy eigenstate, however, interaction-driven screening, which would lead to population at multiple sites, should be present if the interaction strength U is non-negligible at the start of the ramp, which is the case in our experiments. Our initialization procedure thus fails to initialize this screened maximal energy state, and our prepared ES in fact represents a collection of high energy states. Our measurement of critical Δ/J values for the ES that are quantitatively lower than those predicted for the true ES is consistent with nonideal state initialization [43]. Still, our results indicate the observation of a parameter-tunable mobility edge that is influenced by interactions.

Together, our presented experimental data and the simulation results can be viewed as the localization phase diagram for the extremal states of the GAA model with local, attractive mean-field interactions. Because the extremal energy states are the first or final state to undergo a localization transition for increasing Δ , the combined upper and lower boundaries in Fig. 3 can be viewed as defining the critical boundaries for the onset of a mobility edge. This result constitutes the first experimental realization of an exact mobility edge by emulating the generalized Aubry-André model in the presence of interactions [36]. In the future, these results may be extended [53] to allow

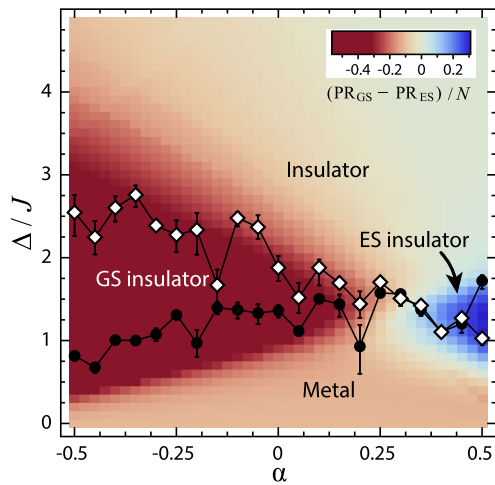


FIG. 3. Localization phase diagram of the GS and ES. Critical quasiperiodicity values for the onset of GS and ES delocalization (filled circles and open diamonds), overlaid on the difference in normalized participation ratio (PR/N , with difference shown according to the inset colorbar) of the numerically calculated extremal eigenstates for a mean-field interaction $U = 0.48J$. The GS and ES transition “lines” do not coincide, indicating a mobility edge, and they cross away from $\alpha = 0$, indicating a shift due to atomic interactions. Vertical error bars denote the 90% confidence intervals of the fit used to determine the critical Δ/J values [43].

the precise determination of the energy of the mobility edge in this and other quasiperiodic models [54], as well as to determine the role of critical wave functions in enhancing interaction effects [55–59].

This material is based upon work supported by the Air Force Office of Scientific Research under Grant No. FA9550-18-1-0082 (F. A. A., E. J. M., and B. G.) and Grant No. FA9550-20-1-0136 (J. H. P.), by the National Science Foundation under Grant No. OMA-1936351 (S. G.), and by NASA under Grant No. SUB JPL 1553869 (K. P. and S. V.).

*These authors contributed equally to this work.

†Present address: Honeywell Quantum Solutions, Golden Valley, Minnesota 55422, USA.

‡sganeshan@ccny.cuny.edu

§jed.pixley@physics.rutgers.edu

¶smivish@illinois.edu

¶bgadway@illinois.edu

- [1] P. W. Anderson, *Phys. Rev.* **109**, 1492 (1958).
- [2] M. Segev, Y. Silberberg, and D. N. Christodoulides, *Nat. Photonics* **7**, 197 (2013).
- [3] L. Sanchez-Palencia and M. Lewenstein, *Nat. Phys.* **6**, 87 (2010).
- [4] Y. Lahini, A. Avidan, F. Pozzi, M. Sorel, R. Morandotti, D. N. Christodoulides, and Y. Silberberg, *Phys. Rev. Lett.* **100**, 013906 (2008).

- [5] G. Roati, C. D’Errico, L. Fallani, M. Fattori, C. Fort, M. Zaccanti, G. Modugno, M. Modugno, and M. Inguscio, *Nature (London)* **453**, 895 (2008).
- [6] L. Fallani, J. E. Lye, V. Guarrera, C. Fort, and M. Inguscio, *Phys. Rev. Lett.* **98**, 130404 (2007).
- [7] S. Aubry and G. André, *Ann. Isr. Phys. Soc.* **3**, 18 (1980).
- [8] D. J. Thouless, *Phys. Rev. Lett.* **61**, 2141 (1988).
- [9] J. Sokoloff, *Phys. Rep.* **126**, 189 (1985).
- [10] K. Drese and M. Holthaus, *Phys. Rev. Lett.* **78**, 2932 (1997).
- [11] C. M. Soukoulis and E. N. Economou, *Phys. Rev. Lett.* **48**, 1043 (1982).
- [12] Y.-Y. Liu, R. Riklund, and K. A. Chao, *Phys. Rev. B* **32**, 8387 (1985).
- [13] D. J. Thouless, *Phys. Rev. Lett.* **61**, 2141 (1988).
- [14] S. Das Sarma, S. He, and X. C. Xie, *Phys. Rev. Lett.* **61**, 2144 (1988).
- [15] S. Das Sarma, S. He, and X. C. Xie, *Phys. Rev. B* **41**, 5544 (1990).
- [16] J. Biddle, B. Wang, D. J. Priour, and S. Das Sarma, *Phys. Rev. A* **80**, 021603(R) (2009).
- [17] J. Biddle and S. Das Sarma, *Phys. Rev. Lett.* **104**, 070601 (2010).
- [18] J. Settimo, N. Lo Gullo, A. Sindona, J. Goold, and F. Plastina, *Phys. Rev. A* **95**, 033605 (2017).
- [19] H. Yao, H. Khoudli, L. Bresque, and L. Sanchez-Palencia, *Phys. Rev. Lett.* **123**, 070405 (2019).
- [20] R. Modak, S. Ghosh, and S. Mukerjee, *Phys. Rev. B* **97**, 104204 (2018).
- [21] D. J. Boers, B. Goedeke, D. Hinrichs, and M. Holthaus, *Phys. Rev. A* **75**, 063404 (2007).
- [22] X. Li, X. Li, and S. Das Sarma, *Phys. Rev. B* **96**, 085119 (2017).
- [23] G. Lemarié, B. Grémaud, and D. Delande, *Europhys. Lett.* **87**, 37007 (2009).
- [24] T. Devakul and D. A. Huse, *Phys. Rev. B* **96**, 214201 (2017).
- [25] J. H. Pixley, J. H. Wilson, D. A. Huse, and S. Gopalakrishnan, *Phys. Rev. Lett.* **120**, 207604 (2018).
- [26] K. Viebahn, M. Sbroscia, E. Carter, J.-C. Yu, and U. Schneider, *Phys. Rev. Lett.* **122**, 110404 (2019).
- [27] M. Sbroscia, K. Viebahn, E. Carter, J.-C. Yu, A. Gaunt, and U. Schneider, *Phys. Rev. Lett.* **125**, 200604 (2020).
- [28] F. Evers and A. D. Mirlin, *Rev. Mod. Phys.* **80**, 1355 (2008).
- [29] F. Jendrzejewski, A. Bernard, K. Mueller, P. Cheinet, V. Josse, M. Piraud, L. Pezzé, L. Sanchez-Palencia, A. Aspect, and P. Bouyer, *Nat. Phys.* **8**, 398 (2012).
- [30] W. R. McGehee, S. S. Kondov, W. Xu, J. J. Zirbel, and B. DeMarco, *Phys. Rev. Lett.* **111**, 145303 (2013).
- [31] G. Semeghini, M. Landini, P. Castilho, S. Roy, G. Spagnolli, A. Trenkwalder, M. Fattori, M. Inguscio, and G. Modugno, *Nat. Phys.* **11**, 554 (2015).
- [32] M. Lopez, J.-F. Clément, P. Szriftgiser, J. C. Garreau, and D. Delande, *Phys. Rev. Lett.* **108**, 095701 (2012).
- [33] H. P. Lüschen, S. Scherg, T. Kohlert, M. Schreiber, P. Bordia, X. Li, S. Das Sarma, and I. Bloch, *Phys. Rev. Lett.* **120**, 160404 (2018).
- [34] F. A. An, E. J. Meier, and B. Gadway, *Phys. Rev. X* **8**, 031045 (2018).
- [35] T. Kohlert, S. Scherg, X. Li, H. P. Lüschen, S. Das Sarma, I. Bloch, and M. Aidelsburger, *Phys. Rev. Lett.* **122**, 170403 (2019).

- [36] S. Ganeshan, J. H. Pixley, and S. Das Sarma, *Phys. Rev. Lett.* **114**, 146601 (2015).
- [37] X. Li, S. Ganeshan, J. H. Pixley, and S. Das Sarma, *Phys. Rev. Lett.* **115**, 186601 (2015).
- [38] X. Li, J. H. Pixley, D.-L. Deng, S. Ganeshan, and S. Das Sarma, *Phys. Rev. B* **93**, 184204 (2016).
- [39] D.-L. Deng, S. Ganeshan, X. Li, R. Modak, S. Mukerjee, and J. H. Pixley, *Ann. Phys. (Berlin)* **529**, 1600399 (2017).
- [40] B. Gadway, *Phys. Rev. A* **92**, 043606 (2015).
- [41] E. J. Meier, F. A. An, and B. Gadway, *Phys. Rev. A* **93**, 051602(R) (2016).
- [42] R. Ozeri, N. Katz, J. Steinhauer, and N. Davidson, *Rev. Mod. Phys.* **77**, 187 (2005).
- [43] See Supplemental Material at <http://link.aps.org/supplemental/10.1103/PhysRevLett.126.040603>, which includes Refs. [44–46], for more details on our determination of the critical Δ/J values for the delocalization transitions, on the adiabaticity of our parameter ramp, on the state initialization procedure, and on the nature of interactions in the synthetic lattice and our and our mean-field calculations that incorporate their effects.
- [44] M. Kohmoto, B. Sutherland, and C. Tang, *Phys. Rev. B* **35**, 1020 (1987).
- [45] H. Hiramoto and M. Kohmoto, *Int. J. Mod. Phys. B* **06**, 281 (1992).
- [46] D.-L. Deng, S. Ganeshan, X. Li, R. Modak, S. Mukerjee, and J. Pixley, *Ann. Phys. (Berlin)* **529**, 1600399 (2017).
- [47] T. Ozawa and H. M. Price, *Nat. Rev. Phys.* **1**, 349 (2019).
- [48] M. Schreiber, S. S. Hodgman, P. Bordia, H. P. Lüschen, M. H. Fischer, R. Vosk, E. Altman, U. Schneider, and I. Bloch, *Science* **349**, 842 (2015).
- [49] F. A. An, E. J. Meier, J. Ang’ong’a, and B. Gadway, *Phys. Rev. Lett.* **120**, 040407 (2018).
- [50] T. Giamarchi, *Quantum Physics in One Dimension*, 1st ed. (Oxford University Press, Oxford, 2003).
- [51] B. Deissler, M. Zaccanti, G. Roati, C. D’Errico, M. Fattori, M. Modugno, G. Modugno, and M. Inguscio, *Nat. Phys.* **6**, 354 (2010).
- [52] S. Flach, in *Nonlinear Optical and Atomic Systems: At the Interface of Physics and Mathematics*, edited by C. Besse and J.-C. Garreau (Springer International Publishing, New York, 2015), pp. 1–48.
- [53] L. W. Cheuk, A. T. Sommer, Z. Hadzibabic, T. Yefsah, W. S. Bakr, and M. W. Zwierlein, *Phys. Rev. Lett.* **109**, 095302 (2012).
- [54] S. V. Rajagopal, T. Shimasaki, P. Dotti, M. Račiūnas, R. Senaratne, E. Anisimovas, A. Eckardt, and D. M. Weld, *Phys. Rev. Lett.* **123**, 223201 (2019).
- [55] M. V. Feigel’man, L. B. Ioffe, V. E. Kravtsov, and E. A. Yuzbashyan, *Phys. Rev. Lett.* **98**, 027001 (2007).
- [56] M. S. Foster and E. A. Yuzbashyan, *Phys. Rev. Lett.* **109**, 246801 (2012).
- [57] I. S. Burmistrov, I. V. Gornyi, and A. D. Mirlin, *Phys. Rev. Lett.* **108**, 017002 (2012).
- [58] M. S. Foster, H.-Y. Xie, and Y.-Z. Chou, *Phys. Rev. B* **89**, 155140 (2014).
- [59] Y.-Z. Chou, Y. Fu, J. H. Wilson, E. J. König, and J. H. Pixley, *Phys. Rev. B* **101**, 235121 (2020).